OBSERVATIONS OF CAVITATING FLOWS

Christopher E. Brennen

California Institute of Technology
Pasadena, Calif. 91125

ABSTRACT

This paper will present a review of some of the recent advances in our understanding of the dynamics and acoustics of cavitating flows. We focus first on the individual events which evolve from a single travelling nucleus and describe observations of the intricate micro-fluid-mechanics which affect both the bubble shape and the subsequent emission of noise. These phenomena have important consequences in terms of their implications for the scaling of cavitation damage and noise. We also present calculations of the interaction between the individual traveling bubbles and the irrotational flow outside of the boundary layer of the headform. Comparisons of predicted and experimentally observed bubble shapes show qualitative agreement but further work is neccessary to understand the details of the interactions between the viscous boundary layer and the bubble.

To model the processes of cavitation inception, noise and damage it is neccessary to generate a model of the cavitation event rate which can then be coupled with the consequences of the individual events. In the second part of this paper we describe recent efforts to connect the observed event rates to the measured distributions of cavitation nuclei in the oncoming stream. Such studies neccessarily raise questions regarding the nuclei distributions in water tunnels and in the ocean and it would seem that we still know little of the nuclei population dynamics in either context. This is illustrated by a few observations of the population dynamics in a particular facility.

The third subject addressed in this paper is the question of the noise produced by an individual travelling cavitation event. It is shown that the distortions in the shape of cavitation bubbles leads to acoustic impulses which are about an order of magnitude smaller than those predicted by the spherical bubble dynamics of the Rayleigh-Plesset equation. However, at the higher cavitation numbers, the upper bound on the experimental impulses scales with speed and size much as one would expect from the spherical bubble analysis. Initially, as the cavitation number is decreased, the impulse increases as expected. But, beyond a certain critical cavitation number, the noise again decreases in contrast to the expected increase. This phenomenon is probably caused by two effects, namely the interaction between events at the higher event densities and the reduction in the impulse due to a change in the dominant type of cavitation event.

From the single event we then move to the larger scale structures and the interactions which occur when the density of the events becomes large and individual bubbles begin to interact. One of the more important interaction phenomena which occur results from the behaviour of a cloud of cavitation bubbles. Most previous theoretical studies of the dynamics of cavitating clouds have been linear or weakly non-linear analyses which have identified the natural frequencies and modes of cloud oscillation but have not, as yet, shown how a cloud would behave during the massively non-linear response in a cavitating flow. We present non-linear calculations which show the development of an inwardly propagating shock wave during the collapse phase of the motion. These observations confirm the earlier speculation of Mørch and his co-workers.

INTRODUCTION

Recent years have seen a significant advance of our understanding of the dynamics and acoustics of cavitating flows and the purpose of this paper will be to attempt to summarize some of the improvements in our knowledge of these hydrodynamic and acoustic phenomena.

We begin by describing the effect of the flow on a single cavitation "event", the term used to denote the processes which follow when an individual cavitating nucleus is convected into a region of low pressure. The pioneering observations of single

events which were made by Knapp (see, for example, Knapp and Hollander 1948) were followed by the analyses of Plesset (1949), Parkin (1952) and others who sought to model these observations of the growth and collapse of a travelling cavitation bubble using Rayleigh's equation for the dynamics of a spherical bubble (Rayleigh 1917). Parkin opined that the lack of agreement between the theory and his experimental observations was due to the neglect of the boundary layer. Rayleigh-Plesset models of travelling bubble cavitation which attempted to incorporate the effects of the boundary layer followed and included the work of Oshima (1961), Van der Walle (1962), Holl and Kornhauser (1970) and Johnson and Hsieh (1966). Like Plesset's and Parkin's original models these improved versions continued to make two assumptions, namely that the bubbles remain spherical (except in the later phase of collapse) and that bubbles or events do not interact with one another. Most of the present paper will focus on the departure from these assumptions which occur in real flows and the consequences of these departures in so far as damage potential and noise emission are concerned.

Observations of real flows demonstrate that even single cavitation bubbles are often far from spherical. Indeed, they may not even be single bubbles but rather a cloud of smaller bubbles. In recent years, it has become clear that departure from sphericity often occurs as a result of the interaction of the bubble with the pressure gradients and shear forces in the flow. We shall begin by examining some of these effects while still assuming that the events are sufficiently far apart in space and time that they do not interact with one another or modify the global liquid flow in any significant way.

Before describing some of the experimental observations of bubble/flow interactions, it is valuable to consider the relative sizes of the cavitation bubbles and the viscous boundary layer. In the flow of a uniform stream of velocity, U, around an object such as a hydrofoil with typical dimension, ℓ, the thickness of the laminar boundary layer near the minimum pressure point will be given qualitatively by $\delta \approx (\nu\ell/U)^{\frac{1}{2}}$ where ν is the kinematic viscosity of the liquid. Parenthetically we note that transition to turbulence usually occurs downstream of the point of minimum pressure and consequently the laminar boundary layer thickness is the appropriate dimension for limited cavitation confined to the immediate neighbourhood of the low pressure region. Moreover, the asymptotic growth rate of a bubble yields a typical maximum bubble radius, R_M, given by

$$R_M \approx 2\ell(-\sigma - C_{pmin}) \qquad (1)$$

where σ is the cavitation number defined as $2(p_\infty - p_v)/\rho U^2$ where p_∞ and p_v are respectively the upstream and vapor pressures and ρ is the liquid density. The coefficient of pressure, C_p, is defined as $2(p - p_\infty)/\rho U^2$ where p is the local pressure in the flow and C_{pmin} denotes the minimum pressure coefficient in the flow. It follows that the ratio of the boundary layer thickness to the maximum bubble radius, δ/R_M, is given approximately by

$$\frac{\delta}{R_M} = \frac{1}{2(-\sigma - C_{pmin})}\left\{\frac{\nu}{\ell U}\right\}^{\frac{1}{2}} \qquad (2)$$

Therefore, provided $(-\sigma - C_{pmin})$ is of the order of 0.1 or greater, it follows that for the high Reynolds numbers, $U\ell/\nu$, which are typical of most of the flows in which cavitation is a problem, the boundary layer is usually much thinner than the typical dimension of the bubble. This does not mean the boundary layer is unimportant. But we can anticipate that those parts of the cavitation bubble furthest from the solid surface will interact with the primarily inviscid flow outside the boundary layer, while those parts close to the solid surface will be affected by the boundary layer and the shear forces associated with it.

When the frequency of cavitation events increases in space or time such that they begin to interact with one another a whole new set of phenomena may be manifest. They may begin to interact hydrodynamically with important consequences for both the global flow and the dynamics and acoustics of the individual bubble. For example, clouds of cavitating bubbles are often shed from a cavitating foil and the coherent dynamics of the cloud can result in a collapse process which has much greater potential for noise production and damage than the individual bubbles would have acting independently (see, for example, Soyama *et al.* 1992).

INDIVIDUAL EVENTS

Some of the early (and classic) observations of individual travelling cavitation bubbles by Knapp and Hollander (1948), Parkin (1952) and Ellis (1952) make mention of the deformation of the bubbles by the flow. But the focus of attention soon shifted to the easier observations of the dynamics of individual bubbles in quiescent liquid

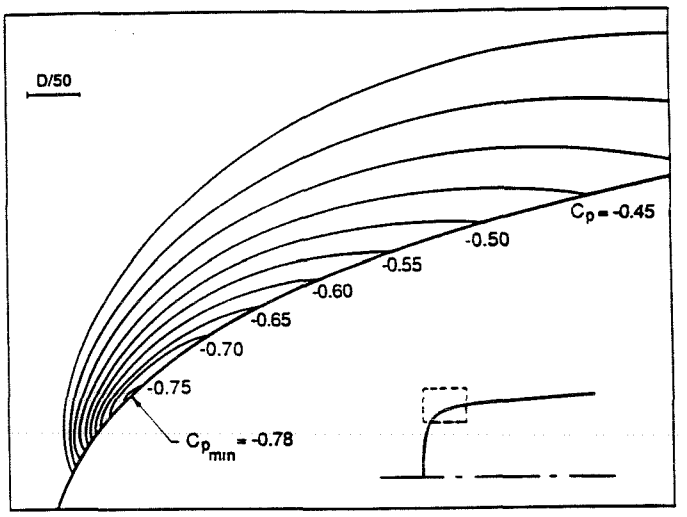

Figure 1: Isobars in the vicinity of the minimum pressure point on the axisymmetric Schiebe headform with values of the pressure coefficient, C_p, as indicated. The pressures were obtained from a potential flow calculation. The insert shows the headform shape and the area that has been enlarged in the main figure (dashed lines). From Schiebe (1972) and Kuhn de Chizelle *et al.* (1992).

and it is only recently that investigations of the deformation caused by the flow have resumed. Both Knapp and Hollander (1948) and Parkin (1952) observed that almost all cavitation bubbles are closer to hemispherical than spherical and that they appear to be separated from the solid surface by a thin film of liquid. Such bubbles are clearly evident in other photographs of travelling cavitation bubbles on a hydrofoil such as those of Blake *et al.* (1977) or Briançon-Marjollet *et al.* (1990).

A number of recent research efforts have focussed on these bubble/flow interactions including the work of van der Meulen and van Renesse (1989) and Briançon-Marjollet *et al.* (1990). Recently, Ceccio and Brennen (1991) and Kuhn de Chizelle *et al.* (1992) have made an extended series of observations of cavitation bubbles in the flow around axisymmetric bodies including studies of the scaling of the phenomena. Two axisymmetric body shapes were used, both of which have been employed in previous cavitation investigations. The first of these was a so-called "Schiebe body" (Schiebe 1972). One of the important characteristics of this shape is that the boundary layer does not separate in the region of low pressure within which cavitation bubbles occur. The second body had the ITTC headform shape which was originally used by Lindgren and Johnsson (1966) and exhibits laminar separation within the region in which the cavitation bubbles occur. For both headforms, the isobars in the neighbourhood of the minimum pressure point exhibit a large pressure gradient normal to the surface as illustrated by the isobars for the Schiebe body shown in figure 1. This pressure gradient is associated with the curvature of the body and therefore the streamlines in the vicinity of the minimum pressure point. Consequently, at a given cavitation number, σ, the region below the vapor pressure which is enclosed between the solid surface and the $C_p = -\sigma$ isobaric surface is long and thin compared with the size of the headform. Only nuclei which pass through this thin volume will cavitate.

The observations of Ceccio and Brennen (1991) at relatively low Reynolds numbers will be described first. Typical photographs of bubbles on the $5.08cm$ diameter Schiebe headform during the cycle of bubble growth and collapse are shown in figure 2. Simultaneous profile and plan views provide a more complete picture of the bubble geometry. In all cases the shape during the initial growth phase was that of a spherical cap, the bubble being separated from the headform surface by a thin layer of liquid of the same order of magnitude as the boundary layer thickness. Later developments depend on the geometry of the headform and the Reynolds number so we begin with the simplest case, namely the Schiebe body at relatively low Reynolds number. Typical photographs for this case are included in figure 2. As the bubble begins to enter the region of adverse pressure gradient the exterior frontal surface begins to be pushed inward

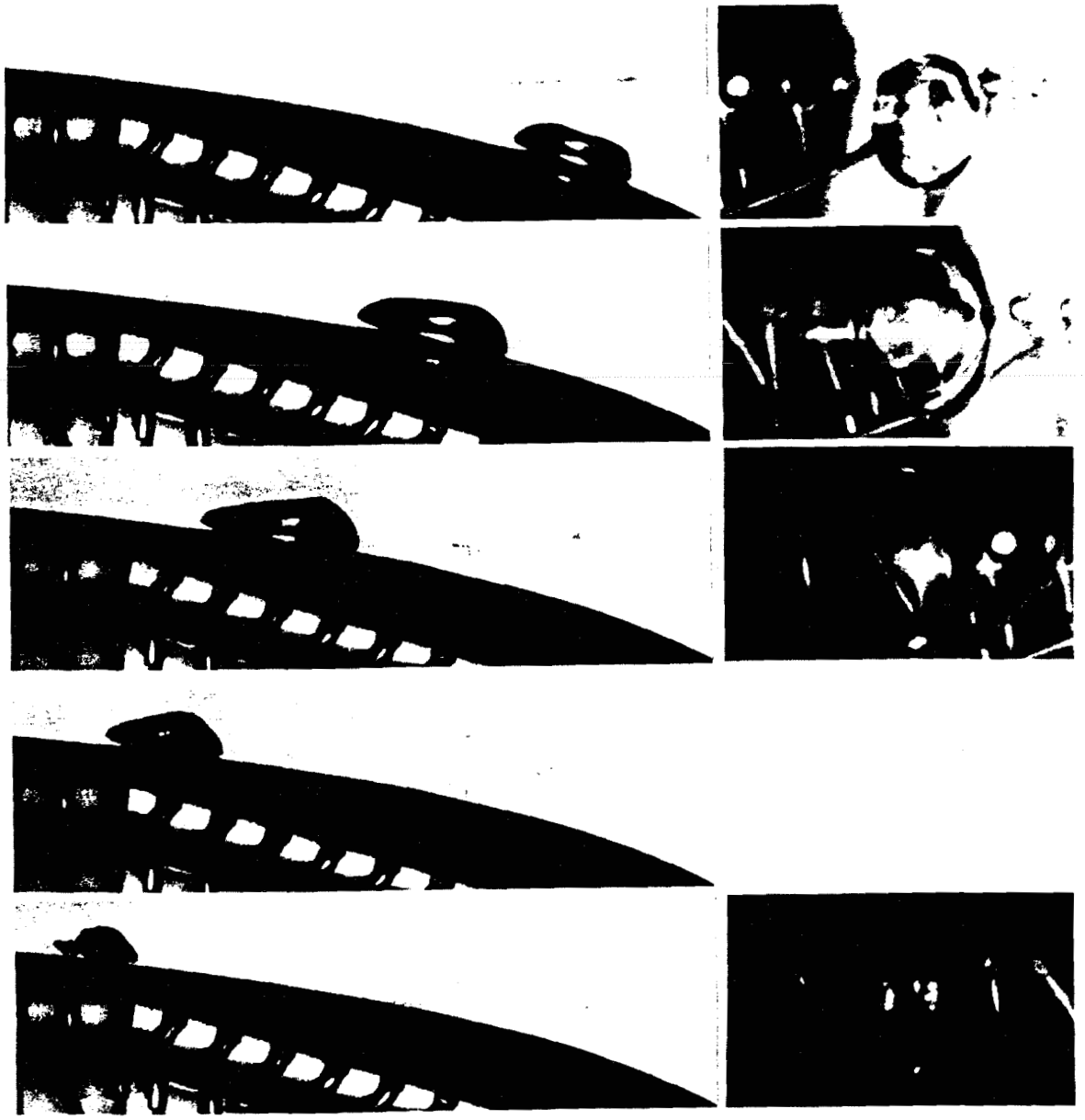

Figure 2: A series of photographs illustrating the growth and collapse of travelling cavitation bubbles in a flow around a $5.08cm$ diameter Schiebe headform at $\sigma = 0.45$ and a speed of 9 m/s. Simultaneous profile and plan views are presented but each row is, in fact, a different bubble. The flow is from right to left. The scale is 4.5 times lifesize. From Ceccio and Brennen (1991).

causing the profile of the bubble to appear wedge-like. Thus the collapse is initiated on the exterior frontal surface of the bubble and this often leads to the bubble fissioning into forward and aft bubbles as seen in figure 2.

But, two other processes are occuring at the same time. First, the streamwise thickness of the bubble decreases faster than its spanwise breadth (spanwise being defined as the direction parallel to the headform surface and normal to the oncoming stream) so that the largest dimension of the bubble is its spanwise breadth. Second, the bubble acquires significant spanwise vorticity through its interactions with the boundary layer during the growth phase. Consequently, as the collapse proceeds this vorticity is concentrated and the bubble

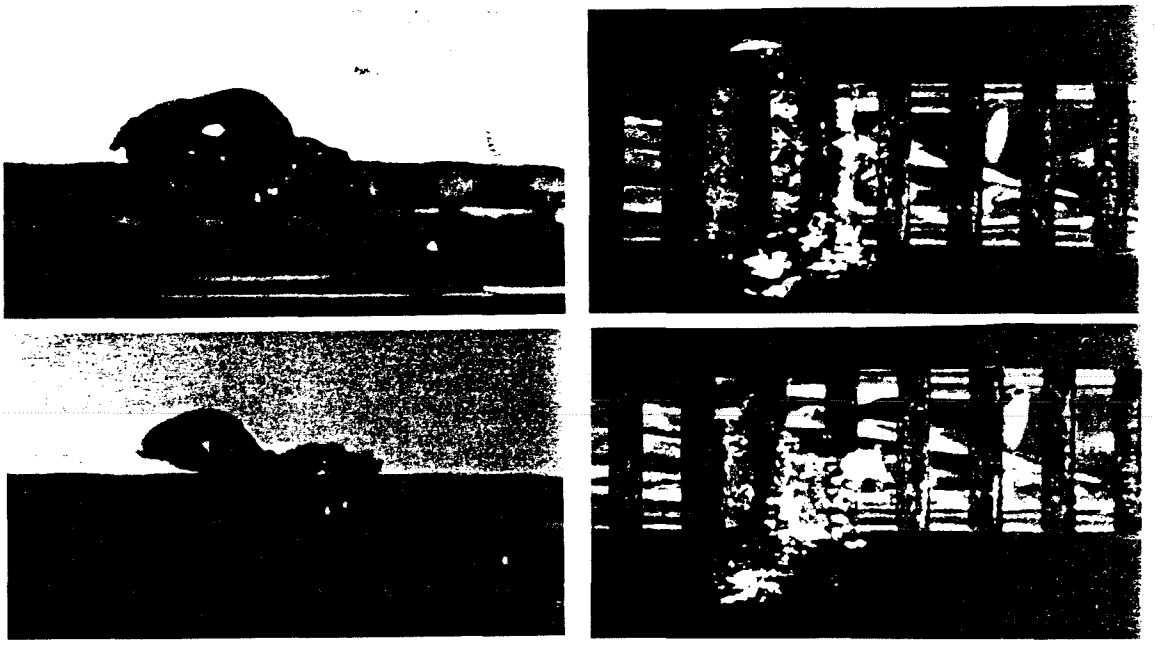

Figure 3: Examples from Ceccio and Brennen (1991) illustrating the instability of the liquid layer under a travelling cavitation bubble (for $\sigma = 0.45$ and a speed of 8.7 m/s). The photographs are 3.8 times lifesize.

evolves into one (or two or possibly more) cavitating vortices with spanwise axes. These vortex bubbles proceed to collapse and seem to rebound as a cloud of much smaller bubbles. Often a coherent second collapse of this cloud was observed when the bubbles were not too scattered by the flow. Ceccio and Brennen (1991) (see also Kumar and Brennen 1993b) conclude that the flow-induced fission prior to collapse can have a substantial effect on the noise impulse.

Two additional phenomena were observed on the headform which exhibited laminar separation, namely the ITTC headform. The first of these was the observation that the layer of liquid underneath the bubble would become disrupted by some instability. As seen in figure 3 this results in a bubbly layer of fluid which subsequently gets left behind the main bubble. Thus the instability of the liquid layer leads to another mechanism of bubble fission. Because of the physical separation, the bubbly layer would collapse after the main body of the bubble.

The second and perhaps more consequential phenomenon observed with the ITTC headform only occurs with the occasional bubble. Infrequently, when a bubble passes the point of laminar separation, it triggers the formation of local "attached cavitation" streaks at the lateral or spanwise extremities of the bubble as seen in figure 4. Then, as the main bubble proceeds downstream, these "streaks" or "tails" of attached cavitation are stretched out behind the main bubble, the trailing ends of the tails being attached to the solid surface. Subsequently, the main bubble collapses first leaving the "tails" to persist for a fraction longer as illustrated by the lower photograph in figure 4.

The importance of these occasional "events with tails" did not become clear until tests were conducted at much higher Reynolds numbers, with larger headforms (up to 50.5cm in diameter) and somewhat higher speeds (up to 15 m/s). These tests were part of an investigation of the scaling of the bubble dynamic phenomena described above (Kuhn de Chizelle *et al.* 1992) which was conducted in the Large Cavitation Channel (LCC, Morgan 1990). One notable observation was the presence of a "dimple" on the exterior surface of all the individual travelling bubbles; examples of this dimple are included in figure 5. They are not the precursor to a re-entrant jet for the dimple seems to be relatively stable during most of the collapse process. More importantly, it was observed that, at higher Reynolds number, "attached tails" occurred even on these Schiebe bodies which did not normally exhibit laminar separation. Moreover, the probability of occurence of attached tails

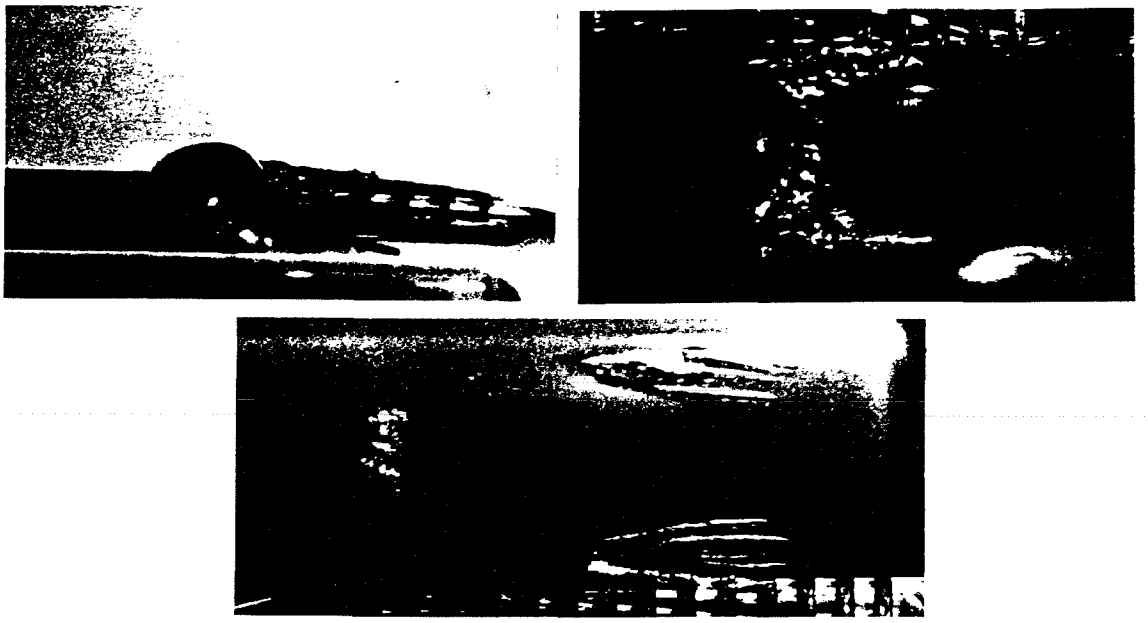

Figure 4: Examples from Ceccio and Brennen (1991) illustrating the attached tails formed behind a travelling cavitation bubble (for $\sigma = 0.42$ and a speed of 9 m/s). The top two are simultaneous profile and plan views. The bottom shows the persistence of the tails after the bubble has collapsed. The photographs are 3.8 times lifesize.

increased as the Reynolds number increased and the attached cavitation began to be more extensive. As the Reynolds number increased further, the bubbles would tend to trigger attached cavities over the entire wake of the bubble as seen in the lower two photographs in figure 5. Moreover the attached cavitation would tend to remain for a longer period after the main bubble had disappeared. Eventually, at the highest Reynolds numbers tested it appeared that the passage of a single bubble was sufficient to trigger a "patch" of attached cavitation (figure 5, bottom) which would persist for an extended period after the bubble had long disappeared. We note that Howison *et al.* (1993) have recently examined an inviscid model for such patch cavities.

This progression of events and the changes in the probabilities of the different kinds of events with Reynolds number imply a rich complexity in the micro-fluidmechanics of cavitation bubbles, much of which remains to be understood. Its importance lies in the fact that these different types of events cause differences in the collapse process which, in turn, alters the noise produced (see Kuhn de Chizelle *et al.* 1992) and, in all probability, the potential for cavitation damage. For example, the events with attached tails were found to produce significantly less noise than the events without tails. Due to the changes in the probabilities of occurence of these events with Reynolds number, this implies a scaling effect which had not been previously recognized. It also suggests some possible strategies for the reduction of cavitation noise and damage.

When examined in retrospect, one can identify many of these phenomena in earlier photographic observations, including the pioneering, high-speed movies taken by Knapp. As previously remarked, Knapp and Hollander (1948), Parkin (1952) and others noted the spherical-cap shape of most travelling cavitation bubbles. The ITTC experiments (Lindgren and Johnsson 1966) emphasized the diversity in the kinds of cavitation events which could occur on a given body and later authors attempted to identify, understand and classify this spectrum of events. For example, Holl and Carroll (1979) observed a variety of different types of cavitation events on axisymmetric bodies and remarked that both travelling and attached cavitation "patches" occurred and could be distinguished from travelling bubble cavitation. A similar study of the different types of cavitation events was reported by Huang (1979) whose "spots" are synonymous with "patches".

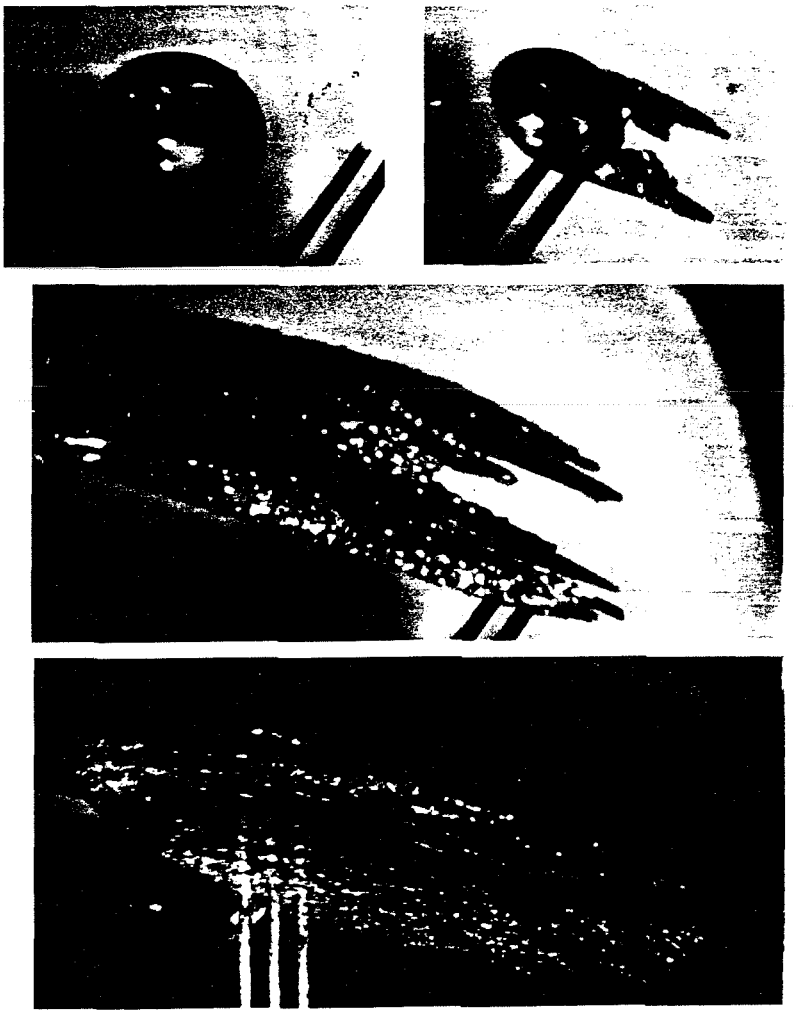

Figure 5: Typical cavitation events from the scaling experiments of Kuhn de Chizelle *et al.* (1992) showing an unattached bubble with "dimple"(upper left), a bubble with attached tails (upper right) and a transient bubble-induced patch (middle) all occuring on the $50.8cm$ diameter Schiebe headform at $\sigma = 0.605$ and a speed of 15 m/s. The bottom photograph shows a patch on the $25.4cm$ headform at $\sigma = 0.53$ and a speed of 15 m/s. The flow is from right to left. The top four are shown at 1.3 times lifesize and the bottom at 1.25 times lifesize.

MODELLING THE BUBBLE DYNAMICS

It is clear that the Rayleigh-Plesset analysis of a spherical bubble cannot reproduce many of the phenomena described in the preceding section. To study this further, Kuhn de Chizelle *et al.* (1994) developed an unsteady numerical code which models the bubbles using travelling sources and incorporates the distortion caused by the pressure gradients in the flow around the body. Only the irrotational flow outside of the boundary layer is addressed so the interaction of the bubble and the boundary layer is not treated by this method. The objective was to focus on the interaction of the bubble with the irrotational flow and the resulting shape of the exterior surface of the bubble. Different, viscous flow analyses would be needed to study the phenomena of the liquid layer instablity and the triggering of attached cavitation.

The basic, simplifying assumption behind the model is that the perturbations in the irrotational flow caused by the bubble can be fairly accurately modelled by a simple travelling source of adjustable intensity and position and that, once an image source is added to substantially satisfy the boundary condition on the headform surface, the remain-

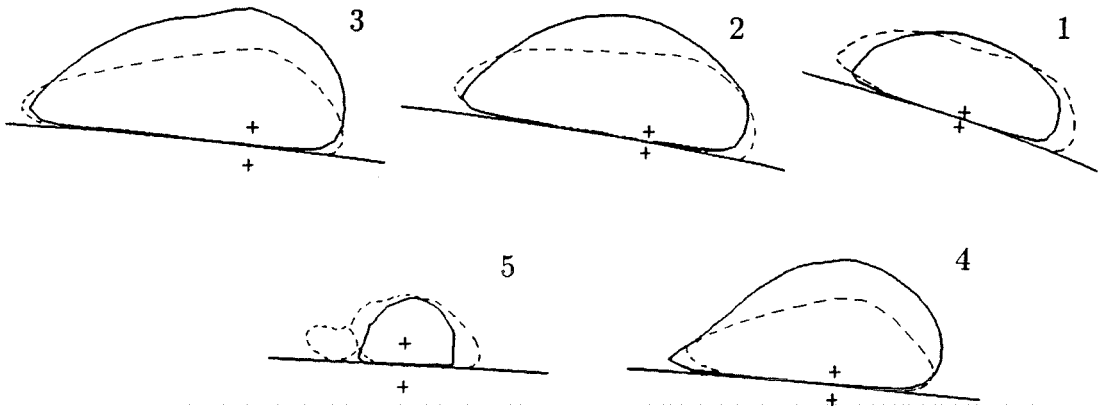

Figure 6: Comparison between the profiles of bubbles in figure 2 (dashed lines) and the profiles calculated by Kuhn de Chizelle *et al.* (1994) (solid lines) at five different moments during growth and collapse, consecutively numbered 1 through 5. The flow is from right to left. The locations of the source and the image source are shown by the crosses.

ing corrections which are required involve small modifications of the basic structure of the flow. It is, of course, possible to solve the inviscid, irrotational problem by using a boundary integral method in which the surface of the headform and the surface of the bubble are divided into boundary elements. Indeed, Chahine (1992) made some preliminary calculations of this kind. However, the travelling source method has the advantage of improved resolution of the bubble dynamics at much reduced computational time. The method could also be extended to allow studies involving more than one bubble so that interaction effects might be examined.

Typical results are presented in figure 6 where the bubble profiles from the photographs of figure 2 are compared with the profiles computed at the same five moments in time (labelled 1 to 5) during the bubble evolution. It can be seen that the overall size of the bubbles are in good agreement with the observations and that there is qualitative agreement in the general shape of the bubble as well as the way it changes with time. The program reproduces the spherical-cap shapes which are separated from the headform by a thin liquid layer. During the growth phase we note a minor depression in the top of the cap which is reminiscent of the dimples on the top of the bubbles observed by Kuhn de Chizelle *et al.* (1992) but is not as pronounced. Later the bubble assumes the wedge-like shape similar to the experiments. The computed bubbles are not, however, as elongated as those observed experimentally, particularly at the higher cavitation numbers; the probable reason for this is that the shape distortions which can be modelled by a single source are limited. Clearly, however, dipoles or higher order models for the bubble would allow more distorted bubble shapes.

One of the advantages of such a calculation is that it allows computation of the unsteady pressure field surrounding the bubble. This allows evaluation of potential interactions between bubbles. By examining the flow perturbations for different cavitation numbers, the potential for bubble/bubble interactions can be evaluated. Moreover, the present method could readily be extended to include a number of simultaneous cavitation events and therefore allow direct evaluation of these interactions.

CAVITATION EVENT RATES

In order to synthesize the cumulative effects of a stream of travelling cavitation bubbles it is neccessary to supplement the details of individual events with the rates at which these events occur. In this section we shift attention to this other aspect of the problem, namely the prediction of the event rate.

Many investigators have anticipated a relationship between the cavitation event rate and the concentration of cavitation nuclei in the oncoming stream (see, for example, Schiebe, 1972, Keller, 1972 and 1974, Keller and Weitendorf, 1976, Kuiper, 1978, Gates and Acosta, 1978). At first sight this seems like a straightforward problem of computing the flux of nuclei into the region for which $C_p < -\sigma$. However many complications

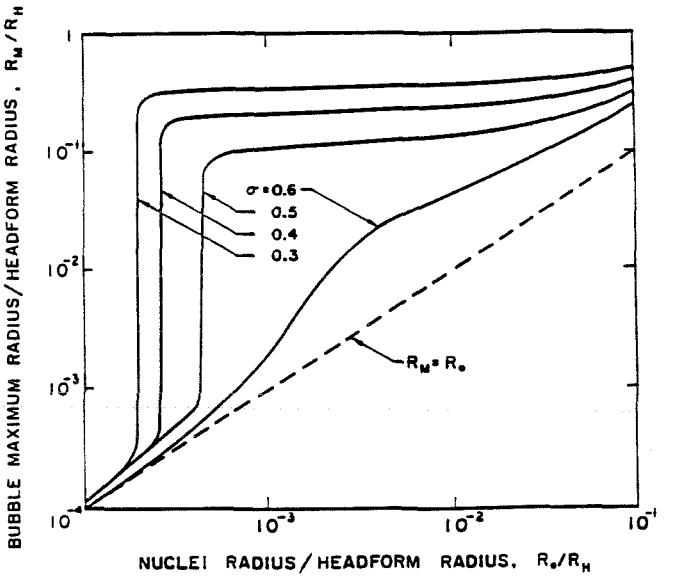

Figure 7: The maximum size, R_M, to which a cavitation bubble grows according to the Rayleigh-Plesset equation as a function of the original nucleus size, R_o, and the cavitation number, σ, in the flow around the Schiebe headform with Weber number, $\rho R_H U^2/S = 28000$.

arise which make this analysis more complex than might otherwise appear and we shall discuss some of the specific issues below. But these difficulties do not account for the lack of experimental research into the relationship. Rather, the difficulties involved in the accurate measurement of the incoming nuclei number distribution function, $N(R)$, have been responsible for the delay in any detailed, quantitative investigation of this component of the problem. By definition, $N(R)dR$ is the number of nuclei with size between R and $R + dR$ per unit volume. As Billet (1985) remarked in his review of nuclei measurement techniques, the only reliable method of obtaining $N(R)$ has been the extremely time consuming method of surveying a reconstruction of an *in situ* hologram of a small volume of tunnel water. However, the time and effort required to construct one $N(R)$ distribution by this method has seriously limited the scope of these investigations.

The recent development of light scattering instruments employing phase doppler techniques (Saffman *et al.* 1984, Tanger *et al.* 1992) has improved the situation. In our own laboratory we have attempted to validate and calibrate a Dantec Phase Doppler Anemometer (PDA) instrument by taking simultaneous measurements with the PDA and a holographic system (Liu *et al.* 1993a). The great advantage of the PDA system is the speed with which $N(R)$ can be measured. After validation, the PDA system could be used with confidence for investigations of the nuclei population dynamics in a water tunnel and of the aforementioned relation between $N(R)$ and the cavitation event rate.

The population dynamics within a facility are important because they determine the rate of change of $N(R)$ with run time and its dependence on tunnel velocity, pressure and air content. However, the dynamics probably vary considerably from one facility to another depending, for example, on whether the facility has a resorber or not. Liu *et al.* (1993a) showed that, in the Low Turbulence Water Tunnel at Caltech (which does not have a resorber), significant variations in $N(R)$ commonly occurred during run times of the order of several minutes though $N(R)$ would asymptote to some steady distribution after about 25 minutes. This "steady state" would not only depend, however, upon the tunnel pressure, velocity and air content but also on the object in the working section and whether or not it was cavitating. This recognition that the nuclei population adjusts to the conditions of the experiment, only serves to emphasize even more strongly the need to monitor $N(R)$ in any cavitation experiment. The role played by a cavitating body (mounted in the working section) in supplying nuclei to the tunnel was

further studied by Sato *et al.* (1993) who examined the distributions at various points in the wake behind a cavitating circular cylinder. In the case examined the nuclei population in the wake was several orders of magnitude larger than in the tunnel as a whole and the process of mixing and diffusion with distance downstream was readily apparent. Recently, Watanabe and Prosperetti (1994) have investigated some simple models for the nuclei created by cavitation and have compared their results with the observations of Sato *et al.*. Clearly, however, more study is required before there is any real understanding of the nuclei population dynamics either in water tunnel facilities or, for that matter, in the ocean (O'Hern *et al.* 1988).

If the nuclei number distribution is known or measured, then the important question is how that determines the cavitation event rate. If the nuclei were to follow the fluid motion without any slip and if the bubble was always spherical and always small relative to the important dimensions of the flow, the problem would be relatively simple. For each streamtube passing close to the body in which nuclei are likely to grow into macroscopic bubbles, one could input the pressure time history into the Rayleigh-Plesset equation and, for a range of initial nuclei sizes and cavitation numbers, calculate the resulting cavitation bubble size history. Such, of course, was the approach taken in the pioneering work of Plesset (1949), Parkin (1952) and others. An example of such a calculation (taken from Ceccio and Brennen, 1991) is shown in figure 7 which presents results from the integration of the Rayleigh-Plesset equation for bubbles in the flow around a Schiebe headform. The maximum size which the bubbles achieve is plotted as a function of the size of the original nucleus for a typical Weber number, $\rho R_H U^2/S$, where U and R_H are the free stream velocity and headform radius and S is the surface tension. Data are plotted for four different cavitation numbers, σ. Note that the curves for $\sigma < 0.5$ all have abrupt vertical sections at certain critical nuclei sizes which correspond to the appropriate Blake critical nuclei sizes (Blake 1949, Daily and Johnson 1956). Since this decreases with decreasing σ an increasing number of smaller nuclei are activated as σ is decreased. The calculations of figure 7 were carried out using the pressure distribution on the surface of the headform. It is clear from figure 1, that the pressure distributions on streamsurfaces further from the headform do not have such low pressures and therefore the Blake critical radius increases with distance from the surface until one reaches a streamline on which there are no nuclei large enough to be activated. Note also from figure 7 that, whatever their initial size, most unstable nuclei grow to roughly the same maximum size. This is because both the asymptotic growth rate and the time available for growth are relatively independent of the size of the original nucleus.

But there are other complications which occur in the actual flow and create more serious problems. First, the boundary layer on the headform surface will clearly have an effect on the volume flux through the low pressure region. Secondly, the relative motion between the nuclei and the liquid can be important. Johnson and Hsieh (1966) included relative motion in their analysis and identified an important phenomenon which occurs when the nuclei experience the large fluid accelerations in the vicinity of the stagnation point. Specifically the nuclei migrate outwards onto streamlines further from the stagnation streamline/body surface as a result of the large centripetal accelerations near the stagnation point. And the larger the nuclei, the larger this shift so that the flow acts as a screen or filter. The larger nuclei which are those most likely to cavitate may, in fact, be so displaced that they no longer experience tension in the low pressure region. Both the boundary layer effect and the screening effect are included in the more recent, numerical calculations of Meyer, Billet and Holl (1992). Liu *et al.* (1993b) have constructed an approximate analytical method of evaluating both of these effects.

Other problems arise because the growing bubble rapidly reaches a size which is comparable to important dimensions such as the height of the isobar, $C_p = -\sigma$, above the headform surface. As a result different parts of the bubble surface are exposed to different pressures and the bubble itself changes the local pressure distribution within the flow. Then it becomes neccessary to resort to a complex procedure such as that described in the preceding section in order to calculate the shape and growth of the bubble. Such analyses, which would take the place of the Rayleigh-Plesset calculations, are too complex for inclusion in the present event rate analyses at least initially. In place of this Liu *et al.* (1993b) have devised a somewhat heuristic treatment of these "finite bubble size" effects which involves an altered, effective trajectory for the bubbles.

Figure 8 presents some of the typical results of the Liu *et al.* analysis applied to a $5.08cm$ Schiebe

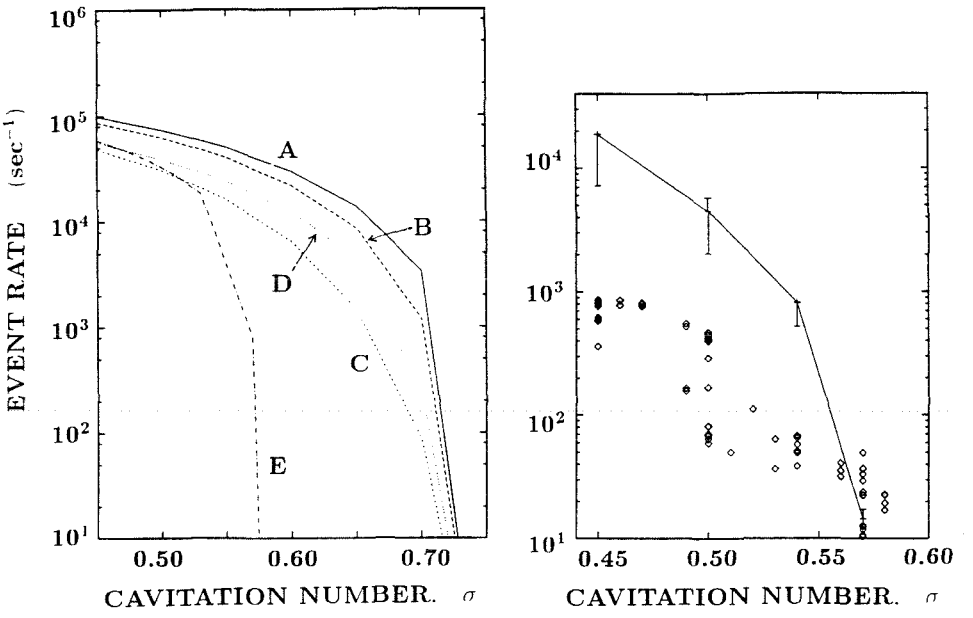

Figure 8: Left: Typical event rates calculated using an assumed but typical nuclei distribution by the method of Liu *et al.* (1993b) for flow around a $5.08cm$ Schiebe body at a velocity of 9 m/s. A: Basic method not including the additional effects included in other lines. B: As A but including the boundary layer flux effect. C: As A but including the bubble screening effect. D: As A but including the surface interference effect. D: As A but including only "observable" bubbles larger than $1mm$ in radius. Right: Comparison of observed cavitation event rates ($\diamond$) on a $5.08cm$ Schiebe body in the LTWT at a speed of 9 m/s with the anticipated event rate based on simultaneously measured nuclei distributions (from Liu and Brennen, 1994).

body at a tunnel speed of 9 m/s. This shows the individual changes in the event rate due to four separate effects, namely the boundary layer flux effect, the screening effect and the finite size effect in the low pressure zone. Also shown is the effect of assuming that the observer will only detect bubbles whose maximum radius is greater than $1mm$. Note that all these effects produce significant alterations in the event rate. Also included in figure 8 is a comparison between experimentally measured event rates and the prediction of the Liu *et al.* method based on the simultaneously measured nuclei distribution. Note that the event rates are in rough agreement at the larger cavitation numbers but that a progressively increasing discrepancy develops as the cavitation number decreases and the event rate increases. At the lowest cavitation numbers this discrepancy is over one order of magnitude. Liu *et al.* surmise that this additional effect is caused by the interaction between nuclei at low cavitation numbers. More explicitly, that many of the smaller nuclei in the liquid surrounding a larger nuclei are not activated because the growth of the larger nuclei generates a sufficient increase in the pressure surrounding the smaller nuclei so that the latter never become unstable.

The scaling effects implicit in both the Meyer *et al.* (1992) and Liu *et al.* (1993b) models provide a qualitative explanation of some of the trends in the experimental observations such as those of Kuhn de Chizelle *et al.* (1994). This is illustrated in figure 9 where data from the LCC experiments of Kuhn de Chizelle *et al.* is presented. Shown on the right in figure 9 are results from the Liu *et al.* model for several speeds and headform sizes using an assumed but typical nuclei distribution function since Kuhn de Chizelle *et al.* were unable to measure the actual distributions in the LCC. Note that changes in the headform size are fairly well modelled whereas changes with tunnel speed are not. The probable explanation is that the changes in tunnel pressure needed to create the same cavitation number at different tunnel speeds result in major changes in the nuclei population in the facility.

Finally we observe that the prediction of the cavitation inception number is inextricably connected with a detailed understanding of the event rate

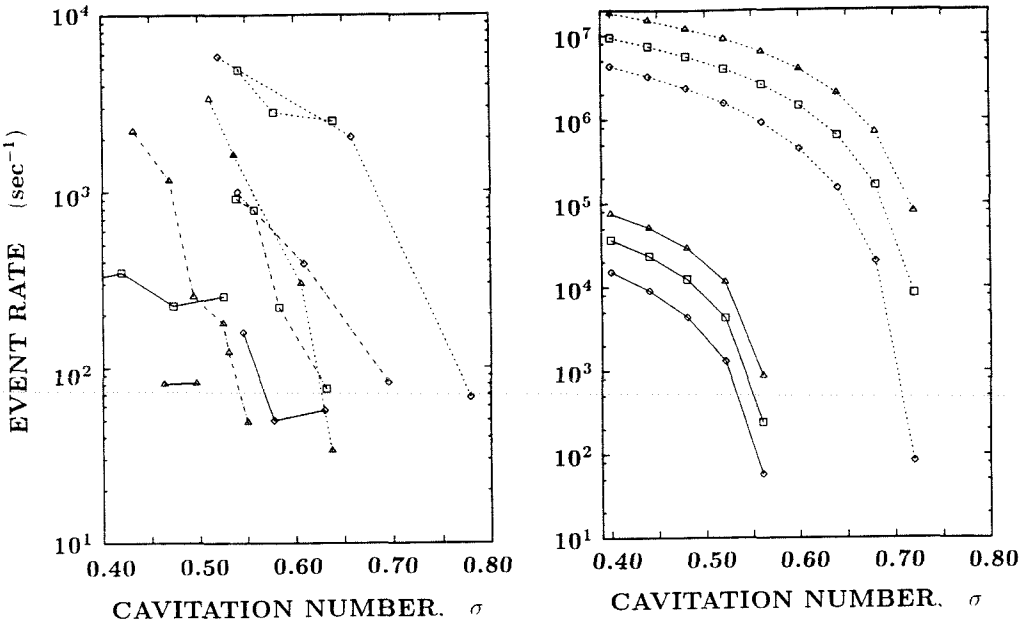

Figure 9: Left: Event rates measured during the scaling experiments of Kuhn de Chizelle *et al.* (1994) in the LCC. Data are shown for three headform diameters ($50.8cm$ = dotted line, $25.4cm$ = dash-dot line, $5.08cm$ = solid line) at three different tunnel velocities ($9m/s$ = $\diamond$, $11.5m/s$ = $\square$, $15m/s$ = $\triangle$). Right: Typical event rates calculated using an assumed but typical nuclei distribution by the method of Liu *et al.* (1993b) for flow around Schiebe bodies of two different sizes ($50.8cm$ = dashed lines, $5.08cm$ = solid lines) for three different velocities ($9m/s$ = $\diamond$, $11.5m/s$ = $\square$, $15m/s$ = $\triangle$). These calculations include the boundary layer flux effect and the screening effect but not the observable size effect.

(Billet and Holl 1979). In figures 10 we make a qualitative comparison between the inception number observed in the LCC experiments of Kuhn de Chizelle *et al.* (1994) and those calculated from the model of Liu *et al.* (1993b) using an assumed but typical nuclei distribution function. Both the observed and calculated σ_i are based on an arbitrarily chosen critical event rate of 50 events per second. In comparing the two graphs in figure 10 we note that the scaling with size is similar while the scaling with speed is quite different probably for the same reason given in the last paragraph.

In conclusion, it seems clear that an adequate model for the event rate is an essential prerequisite for an understanding of cavitation inception (as well as cavitation noise and damage rates).

SINGLE BUBBLE NOISE

With a better understanding of the dynamics of individual cavitation events we now turn to the measurements of the noise produced by those events. In doing so we recognize that noise evaluation provides not only valuable practical information but is also useful as a diagnostic.

The radiated acoustic pressure, p_a, at a large distance, $\mathcal{R}$, from the center of a bubble of volume, $V(t)$, will be given by (Blake 1986)

$$p_a = \frac{\rho}{4\pi\mathcal{R}} \frac{d^2V}{dt^2} \tag{3}$$

It is clear that the noise pulse generated at bubble collapse results from the very large and positive values of d^2V/dt^2 which occur when the bubble is close to its minimum size. A good measure of the magnitude of the collapse pulse is the acoustic impulse, I, defined as the area under the pulse or

$$I = \int_{t_1}^{t_2} p_a dt \tag{4}$$

where t_1 and t_2 are times before and after the pulse at which p_a is zero. It is also useful in the present context to define a dimensionless impulse, I^*, as

$$I^* = 16\pi I\mathcal{R}/\rho U D^2 \tag{5}$$

where $\mathcal{R}$ is now the distance from the cavitation event to the point of noise measurement and D

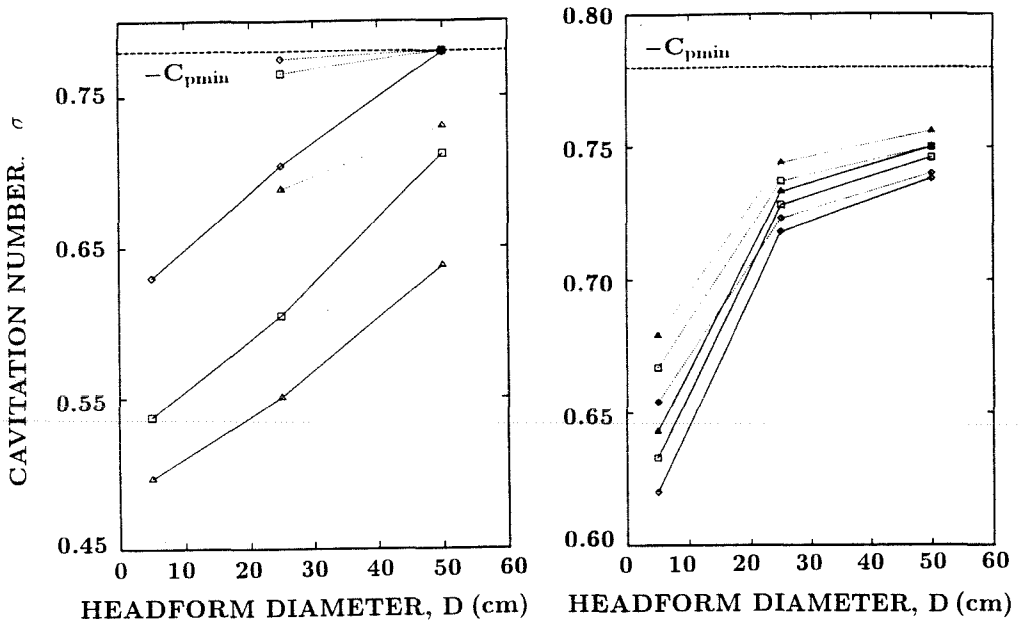

Figure 10: Left: Cavitation inception numbers observed in the scaling experiments of Kuhn de Chizelle *et al.* (1994). Data is shown for three different speeds ($9m/s$ = $\diamond$, $11.5m/s$ = $\square$, $15m/s$ = $\triangle$) and two dissolved oxygen contents (30% = solid lines, 80% = dotted lines) based on a critical event rate of $50s^{-1}$. Right: Predicted cavitation inception numbers at three different speeds ($9m/s$ = $\diamond$, $11.5m/s$ = $\square$, $15m/s$ = $\triangle$) based on a critical event rate of $50s^{-1}$, an assumed but typical nuclei distribution and two minimum observable bubble radii of $1mm$ (solid lines) and $0.5mm$ (dotted lines). From Liu *et al.* (1993b).

is the headform diameter ($D = 2R_H$). We shall compare the experimentally measured values of I^* from individual events on headforms of different size with those from numerical calculations of the growth and collapse of bubbles obtained from integration of the Rayleigh-Plesset equation. Details of these calculations are given in Ceccio and Brennen (1991) and Kuhn de Chizelle *et al.* (1992). For present purposes, we note that variations in the Weber number, Reynolds number and initial size of the nucleus had little effect on the computed impulses (within $\pm 10\%$).

For a range of experimental cavitation numbers, both Ceccio and Brennen (1991) and Kuhn de Chizelle *et al.* (1994) were able to identify within the hydrophone output the signal produced by each cavitation event and to measure the acoustic impulses of these events. The average values of the largest impulses obtained in this way are plotted against cavitation number in figure 11. In viewing this data it must be emphasized that there is considerable variability in the magnitude of the impulses occurring at a particular operating condition. Consequently, the standard deviations corresponding to the averaged I^* values of figure 11 are usually between 25% and 80% of the average value. In both sets of experiments the collapse of an individual bubble (or event) seems to be characterized by a fairly well-defined maximum possible value of the impulse. However the same conditions can also produce impulses which are a fraction of this maximum.

Also shown in figure is a hatched area which encompasses the results from the Rayleigh-Plesset calculations using the pressure distribution on the *surface* of the headform. Note first that the upper envelope of the experimental data for all the headforms and velocities is roughly consistent. However, this envelope of maximum values is approximately one order of magnitude smaller than the impulses obtained from the Rayleigh-Plesset calculations. There are probably two reasons for this. First, the actual maximum volume of the bubbles is significantly smaller than the maximum volume of the Rayleigh-Plesset bubbles as was documented by Kuhn de Chizelle *et al.* (1994). Since the impulse is correlated with the maximum volume, this is clearly one reason for the discrepancy. This effect can be accounted for as will shortly be demonstrated. A more speculative, second reason for the

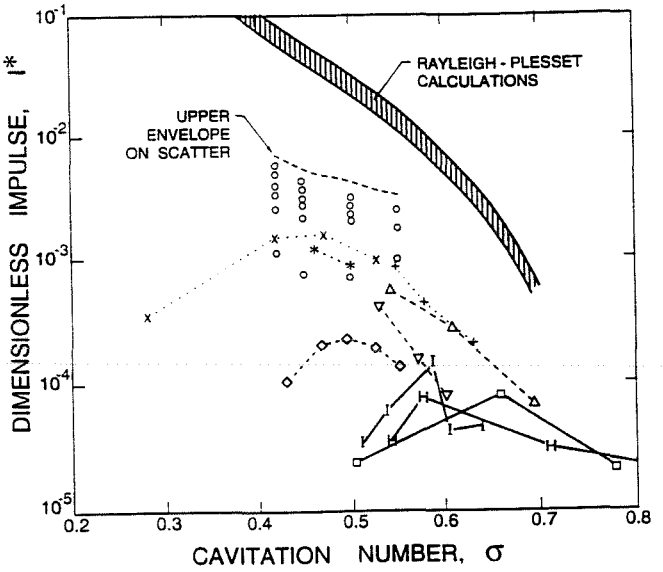

Figure 11: The dimensionless impulse, I^*, as a function of cavitation number, σ. All the calculations using the Rayleigh-Plesset equation lay within the hatched region. The experimental measurements of Ceccio and Brennen (1991) on a $5.08cm$ headform (o) are shown along with the upper envelope which was defined by that data. The results of Kuhn de Chizelle *et al.* (1994) are shown for three headform diameters ($50.8cm$ = thick solid line, $25.4cm$ = thin solid line, $5.08cm$ = dotted line) at three different tunnel velocities ($9m/s$ = +, △, □, $11.5m/s$ = ×, ▽, H, $15m/s$ = ∗, ◇, I).

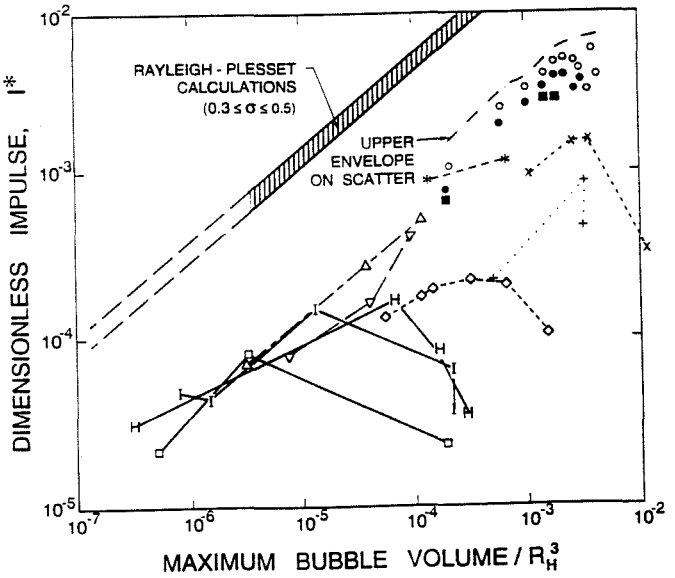

Figure 12: The dimensionless impulse, I^*, as a function of maximum volume of the bubble (divided by $D^3/8$). All the calculations using the Rayleigh-Plesset equation for $0.3 \leq \sigma \leq 0.5$ lie within the hatched region. The experimental measurements on a $5.08cm$ headform by Ceccio and Brennen (1991) are shown for $\sigma = 0.42$ (⊙), 0.45 (•) and 0.50 (solid □) along with the upper envelope which was defined by that data. The results of Kuhn de Chizelle *et al.* (1994) are coded as in figure 11.

discrepancy is that the more non-spherical the collapse, the less noise is produced since a spherical collapse produces the maximum focussing of the unsteady pressures. The interactions of the bubble with the pressure gradients and the boundary layer produce deformations in the shape which, in turn, alter the noise produced.

We speculated that the acoustic impulses would be better correlated with the maximum bubble volume than with the cavitation number. This correlation has been anticipated by many authors including Fitzpatrick and Strasberg (1956), Hamilton *et al.* (1982) and Vogel *et al.* (1989). For this reason Kuhn de Chizelle *et al.* (1994) replotted the impulse data against the maximum cavity volume as shown in figure 12. Note that the correspondence of the upper envelope of the data is improved over that of figure 11, confirming again that the upper bound on the impulse correlates strongly with the maximum bubble volume.

The upper envelope on the experimental data in figure 12 and of the Rayleigh-Plesset calculations are both consistent with a relation of the form

$$I^* \approx \beta \left(\frac{R_{max}}{D} \right)^{\frac{5}{2}} \tag{6}$$

where β is some proportionality constant. There is an explanation for the form of this relation which proceeds as follows. From the definitions given in equations 3, 4 and 5 one can obtain

$$I^* = \frac{4}{UD^2} \left[\left(\frac{dV}{dt} \right)_{t_2} - \left(\frac{dV}{dt} \right)_{t_1} \right] \tag{7}$$

If the typical bubble radius at times t_1 and t_2 is denoted by R_X and the typical pressure coefficient is denoted by C_{px} then it follows from the Rayleigh-Plesset equation (by setting $d^2V/dt^2 = 0$ and evaluating dV/dt) that

$$I^* \approx 32\pi \left(\frac{R_X}{D} \right)^2 (C_{px} - \sigma)^{\frac{1}{2}} \tag{8}$$

Numerical calculations of the Rayleigh-Plesset equation for a wide range of flows and conditions showed that $R_X/R_{max} \approx 0.62$. Moreover calculations with the Schiebe headform pressure distribution showed that $(C_{px} - \sigma) \propto R_{max}/D$. Substituting these two expressions into equation 8 yields the relation 6.

There is, however, another effect which is present in the data of figures 11 and 12. Virtually all of the data for a specific headform size and tunnel velocity tends first to increase as the cavitation number is reduced below the inception value. However, in almost all cases, this trend reaches a maximum at a particular cavitation number (or bubble volume) and begins to decrease with further reduction in σ. There are two effects which may contribute to this phenomenon. First, the noise or impulse may decrease due to the interactions between events as they become more numerous with decreasing σ. Second, the impulse may decrease due to a change in the dominant type of event as σ is decreased. Kuhn de Chizelle *et al.* (1994) showed that the impulses are maximum when the cavities cover about 20% of the surface area of the headform. This is in agreement with the observations of Arakeri and Shanmuganathan (1985) who reported that area void fractions larger than about 25% resulted in significant interactions between the bubbles and a reduction in the acoustic noise. In figure 11, the locations of the maxima appear to be shifted towards higher cavitation numbers at the lower velocities. This trend is consistent with that of Kuhn de Chizelle *et al.* (1994) who found an increase in the area void fraction with decreasing velocity at the same cavitation numbers.

There is, however, an additional effect which causes the observed decrease in the impulse below a certain σ. Kuhn de Chizelle *et al.* (1994) were able to demonstrate that events with tails are more likely to occur as the cavitation number is decreased and that such events produce much less noise, presumably because the tails cause further defocussing of the collapse.

In summary, we find that the micro-fluid-mechanics associated with individual events have an important effect on the noise produced by each event and that changes in the micro-fluid-mechanics with Reynolds number produce previously unrecognized scaling effects. However the overall trends are consistent with those predicted by the Rayleigh-Plesset or Fitzpatrick-Strasberg analysis though the maximum acoustic impulses are about an order of magnitude smaller than those of the spherical bubble analyses.

CLOUD CAVITATION

As a final topic we include a few observations on one of the most important bubble interaction effects. When the frequency of cavitation events increases in space or time such that they begin to interact with one another a whole new set of phenomena may be manifest. They may begin to interact hydrodynamically with important consequences for both the global flow and the dynamics

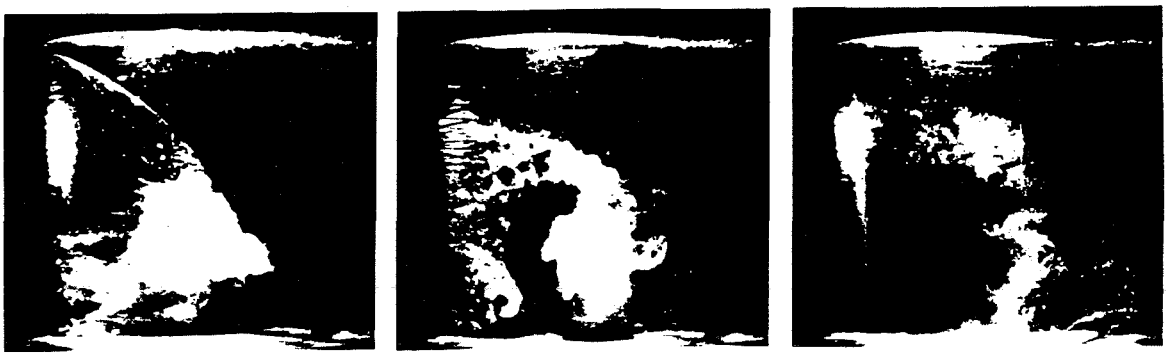

Figure 13: Three frames illustrating the formation, separation and collapse of a cavitation cloud on the suction surface of a hydrofoil ($0.152m$ chord) oscillating in pitch with a frequency of $5.8Hz$ and an amplitude of $\pm 5°$ about a mean incidence angle of 5°. The flow is from left to right, the tunnel velocity is 7.5 m/s and the mean cavitation number is 1.1. Photographs by E. McKenney.

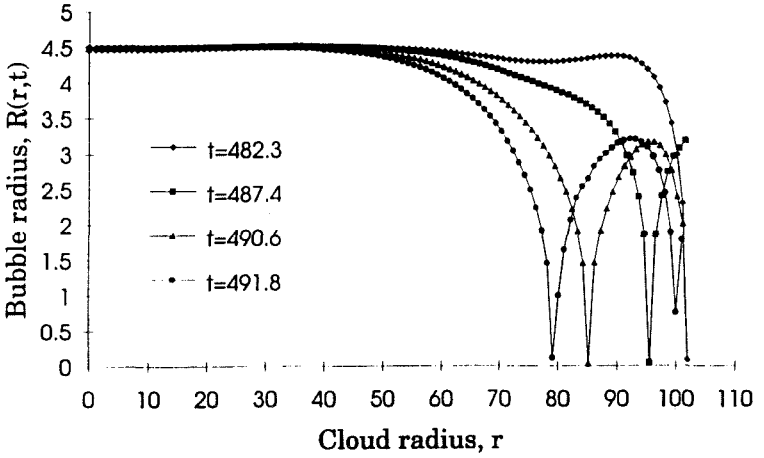

Figure 14: The dimensionless bubble size distribution in the cloud as a function of the dimensionless cloud radius at various times for $\sigma = 0.4$, $C_{pmin} = -0.5$, $\alpha_0 = 0.08\%$, $A_0 = 1cm$, $R_0 = 100\mu m$ and the dimensionless time, $t_G = 500$.

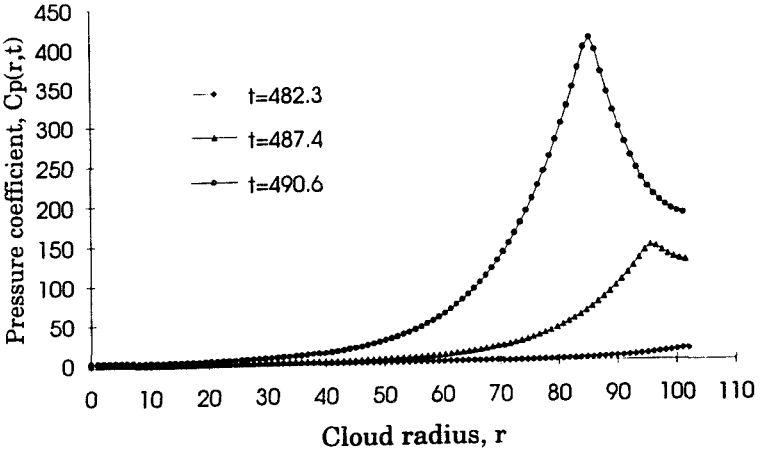

Figure 15: The pressure coefficient distribution in the cloud as a function of the dimensionless cloud radius at various times. Parameters as in figure 14.

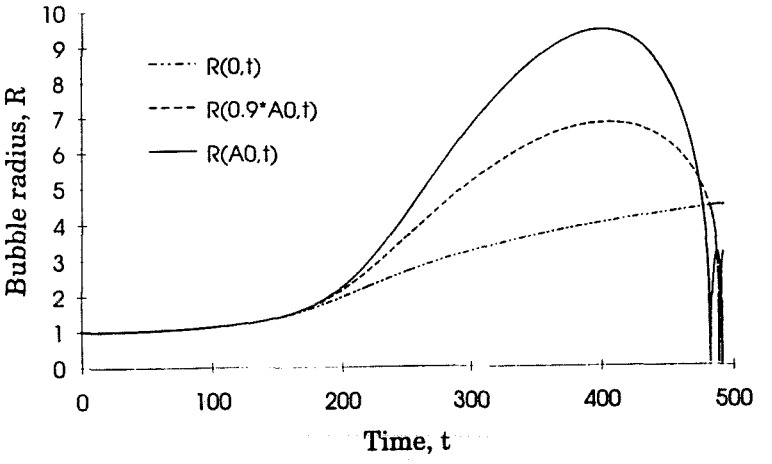

Figure 16: The time history of dimensionless bubble size at three different positions in the cloud, $r_0 = 0$, $r_0 = 0.9A0$ and $r_0 = A0$, where $A0$ is the radius of the cloud. Parameters as in figure 14.

and acoustics of the cavitation. In many flows of practical interest one observes the periodic formation and collapse of a "cloud" of cavitation bubbles. The temporal periodicity may occur naturally as a result of bubble-filled vortices or it may be the response to a periodic disturbance imposed on the flow. Common examples of imposed fluctuations are the interaction between rotor and stator blades in a pump or turbine and the interaction between a ship's propeller and the non-uniform wake created by the hull. In many of these cases the coherent collapse of the cloud of bubbles can cause more intense noise and more potential for damage than in a similar non-fluctuating flow. Bark and van Berlekom (1978), Shen and Peterson (1978), Bark (1985), Franc and Michel (1988) and Kubota *et al.* (1989, 1992) have studied the complicated flow patterns involved in the production and collapse of a cavitating cloud on an oscillating hydrofoil. These studies are exemplified by the photographs of figure 13 which show the formation, separation and collapse of a cavitation cloud on a hydrofoil oscillating in pitch. All of the above mentioned studies emphasize that a substantial bang occurs as a result of the collapse of the cloud; in figure 13 this occurred between the middle and right hand photographs.

Much recent interest has focused on the dynamics and acoustics of finite clouds of cavitation bubbles because of the very destructive effects which are observed to occur when such clouds form and collapse in a flow (see, for example, Bark and van Berlekom 1978, Soyama *et al.* 1992). Here we address the issue of the modelling of the dynamics of cavitation clouds, a subject whose origins can be traced to the work of van Wijngaarden (1964) who first attempted to model the behavior of a collapsing layer of bubbly fluid next to a solid wall. Later investigators explored numerical methods which incorporate the individual bubbles (Chahine 1982) and continuum models which, for example, analyze the behavior of shock waves in bubbly liquid (Noordzij and van Wijngaarden 1974) and identify the natural frequencies of spherical cloud of bubbles (d'Agostino and Brennen 1983). Indeed the literature on the linearized dynamics of clouds of bubbles is growing rapidly (see, for example, Omta 1987, d'Agostino *et al.* 1988 & 1989, Prosperetti 1988). However, apart from some weakly non-linear analyses (Kumar and Brennen 1991, 1992, 1993b) only a few papers have addressed the highly non-linear processes involved during the collapse of a cloud of bubbles. Chahine and Duraiswami (1992) have recently conducted numerical simulations using a number of discrete bubbles and demonstrated how the bubbles on the periphery of the cloud develop inwardly directed re-entrant jets. However, most clouds contain many thousands of bubbles and it therefore is advantageous to examine the non-linear behavior of continuum models.

Another perspective on the subject of collapsing clouds was that introduced by Mørch and his coworkers (Mørch 1980 & 1981, Hanson *et al.* 1981). They speculated that the collapse of a cloud of bubbles involves the formation and inward propagation of a shock wave and that the geometric focusing of this shock at the center of cloud creates the enhancement of the noise and damage potential associated with cloud collapse. Most recently Wang and Brennen (1994) have used the mixture models

employed earlier by d'Agostino *et al.* (1983, 1988, 1989) to study the non-linear growth and collapse of a spherical cloud of bubbles. A finite cloud of nuclei is subjected to a decrease in the ambient pressure which causes the cloud to cavitate and then to a pressure recovery which causes collapse. Of neccessity, the solutions are numerical but they clearly confirm Mørch's vision of cloud collapse. Some typical numerical results are shown in figures 14, 15 and 16. Figures 14 and 15 illustrate the spatial distribution of bubble radius and pressure at several moments in time during the beginning of collapse. Note the formation and inward propagation of a shock wave. The structure of this shock is very similar to those in the bubbly flows investigated by Noordij and van Wijngaarden (1974); it develops a series of rebounds and secondary collapses which probably produce a ringing in the radiated sound. Note also from figure 15 how the pressure pulse increases in amplitude as the shock propagates inwards. Finally, figure 16 presents the time history of bubble size at several Lagrangian locations within the cloud and shows how the bubbles at the cloud surface ($R(A0,t)$) collapse first and shield the interior so that collapse of the interior bubbles is delayed.

Both experimental and analytical studies of this phenomenon are currently being pursued.

CONCLUDING COMMENTS

In this paper we have summarized some of the recent advances in our understanding of travelling bubble cavitation and cloud cavitation. We have demonstrated that it is possible to synthesize the cavitation from knowledge of the nuclei number distribution and the detailed flow field especially that in the neighbourhood of the minimum pressure point. The observations of the dynamics of individual bubbles or events clearly display a rich variety of fluid mechanical phenomena as the bubbles interact with the largely irrotational flow outside the boundary layer and with the boundary layer itself. Many of the observed phenomena remain to be understood, particularly the instability of the thin liquid layer underneath the bubble and the separation phenomena induced by the passage of the bubble. It has been demonstrated that these microfluidmechanical effects are important because they influence the coherence of the collapse and therefore the noise and damage potential which are produced.

We have, of course, omitted any discussion of vortex cavitation or attached cavitation, not because these are less important but rather because the modelling of these forms are less well understood in terms of their noise producing mechanisms and their damage potential. Recent evidence suggest that vortex cavitation and, perhaps, attached cavitation are also affected by the nuclei population and it seems clear that future research should explore that relationship.

ACKNOWLEDGEMENTS

In writing this review, I came to recognize, again, the debt I owe to a series of outstanding graduate students who contributed much of the work described herein. My profound thanks to Luca d'Agostino, Steven Ceccio, Douglas Hart, Sanjay Kumar, Yan Kuhn de Chizelle, Beth McKenney, Zhenhuan Liu, Yi-Chun Wang and Garrett Reisman. As always, my friend and colleague Allan Acosta provided valuable insights and inspiration. I am also deeply grateful for the support of the Office of Naval Research who sponsored much of the research and supported the preparation of this paper under Contract N00014-91-J-1295.

References

[1] Arakeri, V.H. and Shanmuganathan, V., "On the evidence for the effect of bubble interference on cavitation noise," *J. Fluid Mech.*, 1985, Vol. 159, pp. 131-150.

[2] Bark, G. and van Berlekom, W.B., "Experimental investigations of cavitation noise," *Proc. 12th ONR Symp. on Naval Hydrodynamics*, 1978, pp. 470–493.

[3] Bark, G., "Developments of distortions in sheet cavitation on hydrofoils," *Proc. ASME Int. Symp. on Jets and Cavities*, 1985, pp. 215–225.

[4] Billet, M.L. and Holl, J.W., "Scale effects on various types of limited cavitation," *ASME Int. Symp. on Cavitation Inception*, 1979, pp. 11-24.

[5] Billet, M.L., "Cavitation nuclei measurement - a review," *ASME Cavitation and Multiphase Flow Forum Booklet*, 1985, pp. 31–38.

[6] Blake, F.G., "The onset of cavitation in liquids: I," *Acoustics Res. Lab., Harvard Univ., Tech. Memo.*, 1949, No. 12.

[7] Blake, W. K., Wolpert, M. J. and Geib, F. E., "Cavitation noise and inception as influenced by

boundary-layer development on a hydrofoil," *J. Fluid Mech.*, 1977, Vol. 80, pp. 617–640.

[8] Blake, W.K., "Mechanics of flow-induced sound and vibration," Academic Press, 1986.

[9] Briançon-Marjollet, L., Franc, J.P. and Michel, J.M., "Transient bubbles interacting with an attached cavity and the boundary layer," *J. Fluid Mech.*, 1990, Vol. 218, pp. 355–376.

[10] Ceccio, S.L. and Brennen, C.E., "Observations of the dynamics and acoustics of travelling bubble cavitation," *J. Fluid Mech.*, 1991, Vol. 233, pp. 633–660.

[11] Chahine, G.L. Personal communication, 1992.

[12] Chahine, G.L. and Duraiswami, R., "Dynamical interactions in a multibubble cloud," *ASME J. Fluids Eng.*, 1992, Vol. 114, pp. 680-686.

[13] d'Agostino, L. and Brennen, C.E., "On the acoustical dynamics of bubble clouds," *ASME Cavitation and Multiphase Flow Forum*, 1983, pp. 72-75.

[14] d'Agostino, L. and Brennen, C.E., "Acoustical absorption and scattering cross-sections of spherical bubble clouds," *J. Acoust. Soc. of Amer.*, 1988, Vol. 84, No.6, pp. 2126–2134.

[15] d'Agostino, L. and Brennen, C.E., "Linearized dynamics of spherical bubble clouds," *J. Fluid Mech.*, 1989, Vol. 199, pp. 155-176.

[16] Daily, J.W. and Johnson, V.E., Jr., "Turbulence and boundary layer effects on cavitation inception from gas nuclei," *Trans. ASME*, 1956, Vol. 78, pp. 1695–1706.

[17] Ellis, A.T., "Observations on cavitation bubble collapse," *Calif. Inst. of Tech. Hydr. Lab. Rep.*, 1952, No. 21-12.

[18] Fitzpatrick, H.M. and Strasberg, M., "Hydrodynamic sources of sound," *Proc. First ONR Symp. on Naval Hydrodynamics*, 1956, pp. 241-280.

[19] Franc, J.P. and Michel, J.M., "Unsteady attached cavitation on an oscillating hydrofoil," *J. Fluid Mech.*, 1988, Vol. 193, pp. 171–189.

[20] Gates, E.M. and Acosta, A.J., "Some effects of several free-stream factors on cavitation inception on axisymmetric bodies," *Proc. 12th ONR Symp. on Naval Hydrodynamics*, 1978, pp. 86–108.

[21] Hamilton, M.F., Thompson, D.E. and Billet, M.L., "An experimental study of traveling bubble cavitation and noise," *Proc. ASME Int. Symp. on Cavitation Noise*, 1982, pp. 25-33.

[22] Hanson, I., Kedrinskii, V.K. and Mørch, K.A., "On the dynamics of cavity clusters," *J. Appl. Phys.*, 1981, Vol. 15, pp. 1725-1734.

[23] Holl, J.W. and Kornhauser, A.L., "Thermodynamic effects on desinent cavitation on hemispherical nosed bodies in water at temperatures from $80°F$ to $260°F$," *ASME J. Basic Eng.*, 1970, Vol. 92, pp. 44–58.

[24] Holl, J.W. and Carroll, J.A., "Observations of the various types of limited cavitation on axisymmetric bodies," *Proc. ASME Int. Symp. on Cavitation Inception*, 1979, pp. 87–99.

[25] Howison, S.D., Morgan, J.D. and Ockendon, J.R., "Patch cavitation in flow past a rigid body," *Proc. IUTAM Symp. on Bubble Dynamics and Interface Phenomena, Birmingham, England.*, 1993.

[26] Huang, T.T., "Cavitation inception observations on six axisymmetric headforms," *Proc. ASME Int. Symp. on Cavitation Inception*, 1979, pp. 51–61.

[27] Johnson, V.E., Jr., and Hsieh, T., "The influence of the trajectories of gas nuclei on cavitation inception," *Proc. 6th ONR Symp. on Naval Hydrodynamics*, 1966, pp. 163–182.

[28] Keller, A.P., "The influence of the cavitation nucleus spectrum on cavitation inception, investigated with a scattered light counting method," *ASME J. Basic Eng.*, 1972, pp. 917–925.

[29] Keller, A.P., "Investigations concerning scale effects of the inception of cavitation," *Proc. I.Mech.E. Conf. on Cavitation*, 1974, pp. 109–117.

[30] Keller, A.P. and Weitendorf, E.A., "Influence of undissolved air content on cavitation phenomena at the propeller blades and on induced hull pressure amplitudes," *Proc. IAHR Symp. on Two Phase Flow and Cavitation in Power Generation Systems*, 1976, pp. 65–76.

[31] Knapp, R.T. and Hollander, A., "Laboratory investigations of the mechanisms of cavitation," *Trans. ASME*, 1948, Vol. 70, p. 419.

[32] Kubota, A., Kato, H., Yamaguchi, H. and Maeda, M., "Unsteady structure measurement of cloud cavitation on a foil section using conditional sampling," *ASME J. Fluids Eng.*, 1989, Vol. 111, pp. 204–210.

[33] Kubota, A., Kato, H. and Yamaguchi, H., "A new modelling of cavitating flows - a numerical study of unsteady cavitation on a hydrofoil section" *J. Fluid Mech.*, 1992, Vol. 240, pp. 59–96.

[34] Kuhn de Chizelle, Y., Ceccio, S.L., Brennen, C.E. and Gowing, S., "Scaling experiments on the dynamics and acoustics of travelling bubble cavitation," *Proc. 3rd I.Mech.E. Int. Conf. on Cavitation, Cambridge, England*, 1992, pp. 165–170.

[35] Kuhn de Chizelle, Y., Ceccio, S.L., Brennen, C.E. and Shen, Y., "Cavitation scaling experiments with headforms: bubble acoustics," *Proc. 19th Symp. on Naval Hydrodynamics, Seoul, Korea*, 1992, pp. 72–84.

[36] Kuhn de Chizelle, Y., Ceccio, S.L. and Brennen, C.E., "Observations, scaling and modelling of travelling bubble cavitation", submitted for publication, 1994.

[37] Kuiper, G., "Scale effects on propeller cavitation inception," *Proc. 12th ONR Symp. on Naval Hydrodynamics*, 1978, pp. 400–429.

[38] Kumar, S. and Brennen, C.E., "Non-linear effects in the dynamics of clouds of bubbles," *J. Acoust. Soc. Am.*, 1991, Vol. 89, pp. 707-714.

[39] Kumar, S. and Brennen, C.E., "Harmonic cascading in bubble clouds," *Proc. Int. Symp. on Propulsors and Cavitation, Hamburg*, 1992, pp. 171-179.

[40] Kumar, S. and Brennen, C.E., "A study of pressure pulses generated by travelling bubble cavitation," *J. Fluid Mech.*, 1993a, Vol. 255, pp. 541–564.

[41] Kumar, S. and Brennen, C.E., "Some nonlinear interactive effects in bubbly cavitating clouds," *J. Fluid Mech.*, 1993b, Vol. 253, pp. 565-591.

[42] Lindgren, H. and Johnsson, C.A., "Cavitation inception on headforms. ITTC comparative experiments," *Proc. 11th Int. Towing Tank Conf.*, 1966, pp. 219-232.

[43] Liu, Z., Sato, K. and Brennen, C.E., "Cavitation nuclei population dynamics in a water tunnel," *ASME Cavitation and Multiphase Flow Forum*, 1993a, FED-Vol.153, pp. 119–125.

[44] Liu, Z., Kuhn de Chizelle, Y. and Brennen, C.E., "Cavitation event rates and nuclei distributions," *Proc. ASME Symp. on Cavitation Inception*, 1993b, FED-Vol.177, pp. 13–24.

[45] Liu, Z. and Brennen, C.E., "The relation between the nuclei population and the cavitation event rate for cavitation on a Schiebe body," *Proc. ASME Symp. on Cavitation and Gas Liquid Flows in Fluid Machinery*, 1994.

[46] Meyer, R.S., Billet, M.L. and Holl, J.W., "Freestream nuclei and traveling-bubble cavitation," *ASME J. Fluids Eng.*, 1989, Vol. 114, pp. 672–679.

[47] Mørch, K.A., "On the collapse of cavity cluster in flow cavitation," *Proc. First Int. Conf. on Cavitation and Inhomogenieties in Underwater Acoustics, Springer Series in Electrophysics*, 1980, Vol. 4, pp. 95-100.

[48] Mørch, K.A., "Cavity cluster dynamics and cavitation erosion," *Proc. ASME Cavitation and Polyphase Flow Forum*, 1981, pp. 1-10.

[49] Morgan, W.B., "David Taylor Research Center's Large Cavitation Channel," *Proc. Int. Towing Tank Conference, Madrid, Spain.*, 1990.

[50] Noordij, L. and van Wijngaarden, L., "Relaxation effects, caused by relative motion, on shock waves in gas-bubble/liquid mixtures," *J. Fluid Mech.*, 1974, Vol. 66, pp. 115-143.

[51] O'Hern, T., D'Agostino, L. and Acosta, A.J., "Comparison of holographic and counter measurements of cavitation nuclei in the ocean," *ASME J. Fluids Eng.*, 1988, Vol. 110, pp. 200-207.

[52] Omta, R., "Oscillations of a cloud of bubbles of small and not so small amplitude," *J. Acoust. Soc. Am.*, 1987, Vol. 82, pp. 1018-1033.

[53] Oshima, R., "Theory of scale effects on cavitation inception on axially symmetric bodies," *ASME J. Basic Eng.*, 1961, Vol. 83, pp. 379–398.

[54] Parkin, B.R., "Scale effects in cavitating flow," *Ph.D. Thesis, Calif. Inst. of Tech.*, 1952.

[55] Plesset, M.S., "The dynamics of cavitation bubbles," *ASME J. Appl. Mech.*, 1949, Vol. 16, pp. 228-231.

[56] Prosperetti, A., "Bubble-related ambient noise in the ocean," *J. Acoust. Soc. Am.*, 1988, Vol. 84, pp. 1042-1054.

[57] Rayleigh, Lord (Strutt, John William), "On the pressure developed in a liquid during the collapse of a spherical cavity," *Phil. Mag.*, 1917, Vol. 34, pp. 94–98.

[58] Saffman, M., Buchhave, P. and Tanger, H., "Simultaneous measurements of size, concentration and velocity of spherical particles by a laser doppler method," *Proc. 2nd Int. Symp. on Applications of Laser Anemometry to Fluid Mechanics, Lisbon*, 1984.

[59] Sato, K., Liu, Z. and Brennen, C.E., "The microbubble distribution in the wake of a cavitating circular cylinder," *ASME Cavitation and Multiphase Flow Forum*, 1993, FED-Vol.153, pp. 75–80.

[60] Schiebe, F.R., "Measurements of the cavitation susceptibility of water using standard bodies," *St. Anthony Falls Hydr. Lab., U. of Minnesota*, Rep. No. 118., 1972.

[61] Shen, Y. and Peterson, F.B., "Unsteady cavitation on an oscillating hydrofoil," *Proc. 12th ONR Symp. on Naval Hydrodynamics*, 1978, pp. 362–384.

[62] Soyama, H., Kato, H. and Oba, R., "Cavitation observations of severely erosive vortex cavitation arising in a centrifugal pump," *Proc. Third I.Mech.E. Int. Conf. on Cavitation*, 1992, pp. 103-110.

[63] Tanger, H. and Weitendorf, E.A., "Applicability tests for the phase doppler anemometer for cavitation nuclei measurements," *ASME J. Fluids Eng.*, 1992, Vol. 114, pp. 443–449.

[64] van der Meulen, J. H. J. and van Renesse, R. L., "The collapse of bubbles in a flow near a boundary," *Proc. 17th ONR Symp. on Naval Hydrodynamics, The Hague*, 1989, pp. 195–217.

[65] van der Walle, F., "On the growth of nuclei and related scaling factors in cavitation inception," *Proc. 4th ONR Symp. on Naval Hydrodynamics*, 1962.

[66] van Wijngaarden, L., "On the collective collapse of a large number of gas bubbles in water," *Proc. 11th Int. Conf. Appl. Mech.*, Springer-Verlag, Berlin, 1964, pp. 854-861.

[67] Vogel, A., Lauterborn, W. and Timm, R., "Optical and acoustic investigations of dynamics of the laser-produced cavitation bubbles near a solid boundary layer," *J. Fluid Mech.*, 1989, Vol. 206, pp. 299-338.

[68] Wang, Y.-C. and Brennen, C.E., "Shock wave development in the collapse of a cloud of bubbles," *ASME Cavitation and Multiphase Flow Forum*, 1994.

[69] Watanabe, M. and Prosperetti, A., "The effect of gas diffusion on the nuclei population downstream of a cavitation zone," *Proc. ASME Symp. on Cavitation and Gas Liquid Flows in Fluid Machinery*, 1994.